Preparation of compact biocompatible quantum dots using multicoordinating molecular-scale ligands based on a zwitterionic hydrophilic motif and lipoic acid anchors

Naiqian Zhan, Goutam Palui & Hedi Mattoussi

Department of Chemistry and Biochemistry, Florida State University, Tallahassee, Florida, USA. Correspondence should be addressed to H.M. (mattoussi@chem.fsu.edu).

Published online 14 May 2015; doi:10.1038/nprot.2015.050

Luminescent quantum dots (QDs) can potentially be used for many biological experiments, provided that they are constructed in such a way as to be stable in biological matrices. Furthermore, QDs that are compact in size and easy to couple to biomolecules can be readily used for applications ranging from protein tracking to vasculature imaging. In this protocol, we describe the preparation of ligands comprising either one or two lipoic acid (LA) groups chemically linked to a zwitterion moiety. These ligands are then used to functionalize luminescent QDs via a photochemical transformation of LA. This route produces nanocrystals that are compact in size and stable over a broad range of conditions. In addition, the resulting QDs are readily self-assembled with polyhistidine-appended proteins. This mode of conjugation maintains the protein biological activity and its orientation, yielding highly promising fluorescent conjugates that can be used for imaging and sensing. The protocol in its entirety can be completed in 3 weeks.

INTRODUCTION

Interest in integrating QDs with biological systems is motivated by the great potential that the resulting hybrid platforms offer for advancing our understanding of several complex and highly relevant problems in biology. These platforms can exploit several unique photophysical properties of QDs, including narrow bands of emission wavelengths that are size- and composition-tunable, broad absorption with a high extinction coefficient, and superior photostability and chemical stability compared with organic dyes and fluorescent proteins[1–5]. This permits the efficient excitation of multiple-color QDs with a single light source (single wavelength). QDs also exhibit large two-photon fluorescence emission, with absorption action cross-section ~2–3 orders of magnitude larger than those measured for conventional dyes[6]. These properties make QDs ideally suitable for multicolor *in vivo* imaging and sensing, in which deep-tissue penetration is required[6–8].

The use of QDs in biological applications requires access to aqueous dispersions of nanocrystals that exhibit colloidal stability over a broad pH window and in the presence of elevated concentrations of electrolytes and naturally occurring reducing agents. High-quality QDs with reduced size dispersity and high photoemission quantum yields have thus far been grown via the pyrolysis of organometallic precursors in hot coordinating solvents[9,10]. As prepared, these QDs are capped with a mixture of hydrophobic ligands such as trioctylphosphine/trioctylphosphineoxide (TOP/TOPO), alkylamines and phosphonic acids, and they are dispersible only in organic media (e.g., hexane or toluene)[9–13]. Thus, postsurface modification is required to render the nanocrystals hydrophilic and biocompatible (namely, stable in biological matrices and ultimately nontoxic to cells and tissues). In addition, designing surface functionalization schemes that provide nanocrystals with overall small sizes and that can be easily conjugated to biomolecules (such as proteins and peptides) are highly desired. Indeed, several applications in biology require specific targeting to cell receptors and tissue and the ability of the nanoprobe to access confined spaces within cells and in the blood vasculature[14–16].

Over the past decade, several strategies have been developed to promote the transfer of QDs to buffer solutions[17–23]. One of the strategies that can achieve the above goals is ligand exchange with multicoordinating molecules[18,20]. This route relies on the removal of the native cap from the QD surface and its replacement with bifunctional ligands (either molecular scale or polymeric). It can provide more compact nanocrystals, and furthermore it allows easy introduction of reactive groups onto the QD surface. This is realized using tailor-made bifunctional ligands that contain an anchoring group at one end, for coordination onto the nanocrystal surface, and a chemically reactive group at the other end for further coupling. As ligand-to-metal binding is driven by coordination interactions, its strength depends on the nature of the anchors and the coordination number[21,22,24]. Multidentate anchors are expected to form more stable ligand-to-nanocrystal interactions.

In particular, cap exchange with ligands presenting dihydrolipoic acid anchors combined with poly(ethylene glycol) (DHLA-PEG) has been shown to provide better colloidal stability than PEG-free ligands or ligand-bearing mono-thiol anchoring groups[18,25–28]. An alternative design to enhance the coordination interactions with the nanocrystal surface relied on introducing a few DHLA or histidine groups along a polymer chain; this approach is particularly beneficial when using histidine, as coordination of the imidazole group onto metal surfaces is weaker than that of thiol and other groups[29–32].

PEG has been widely used as a means of providing biocompatibility to various materials (such as dyes, polymers and various nanoparticles), owing to its hydrophilic and relatively inert nature[5,33,34]. For example, we have shown that appending a short PEG chain onto LA anchor(s) provides molecular-scale ligands that can be used to promote colloidal stability of semiconductor QDs and gold nanoparticles in buffer solutions

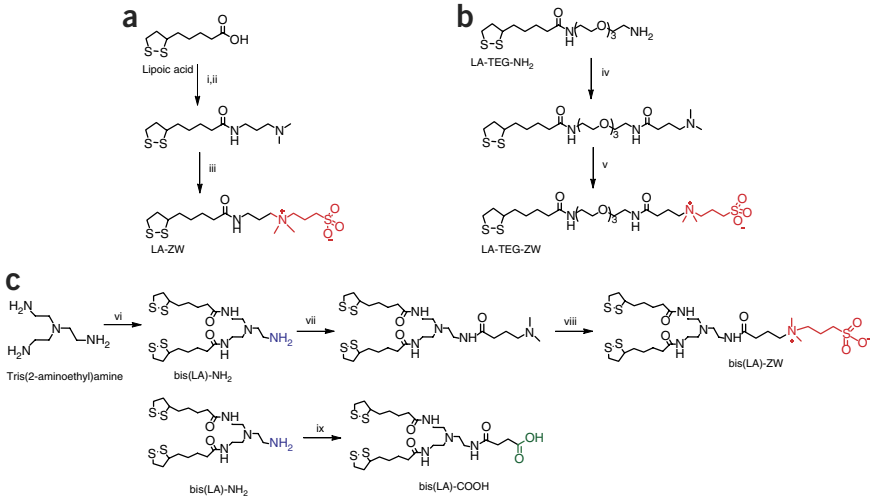

Figure 1 | Schematic description of the synthetic routes used to prepare the various zwitterion ligands used in this report, along with their chemical structures. (**a**–**c**) Synthesis of lipoic acid derivatives (LA)-ZW (**a**), LA-TEG-ZW (**b**) and bis(LA)-ZW (**c**). The steps involved for each reaction are as follows: (i) methanesulfonyl chloride (MsCl), Et_3N and CH_2Cl_2; (ii) *N*,*N*-dimethyl-1,3-propanediamine, Et_3N and CH_2Cl_2; (iii) 1,3-propanesultone and $CHCl_3$; (iv) 4-(dimethylamino)butyric acid hydrochloride, Et_3N, DCC, DMAP and $CHCl_3$; (v) 1,3-propanesultone and $CHCl_3$; (vi) LA, CDI and $CHCl_3$; (vii) *N*,*N*-dimethylaminobutyric acid hydrochloride, Et_3N, DCC, DMAP and $CHCl_3$; (viii) 1,3-propanesultone and $CHCl_3$; and (ix) succinic anhydride, Et_3N and $CHCl_3$. (**a**,**b**) Adapted with permission from ref. 41. (**c**) Adapted from ref. 40 with permission from the American Chemical Society.

while reducing nonspecific interactions[35]. In addition, attaching a terminally reactive group onto the PEG permits conjugation of target molecules onto the nanoparticles[21,26,29,30,36]. However, using a PEG coating prevents self-assembly of full-size proteins appended with a polyhistidine (His_n) tail onto the nanoparticles driven by metal-histidine conjugation; the PEG shell shields the QD surface, and it prevents direct access of the polyhistidine (His_n) tail to the metal-rich surface. The use of this mode of conjugation is useful owing to its simplicity and the fact that proteins are routinely expressed with a C- or N-terminal polyhistidine tag to allow postpreparation purification using Ni-nitrilotriacetic acid (NTA) gel chromatography[37,38]. More recently, several groups have explored the use of zwitterion groups as a potentially more effective means of promoting biocompatibility and drastically reducing uncontrolled agglomeration of nanoparticles in the protein-rich serum and growth medium[28,39]. Furthermore, the zwitterion, being molecular in nature, can drastically reduce the hydrodynamic size of the nanocrystals.

In this report, we describe how to prepare three sets of multicoordinating zwitterion ligands—one set contains one dithiolane group; the second set has one LA (dithiolane moiety) attached to a tetraethylene glycol (TEG) bridge; and the third set contains two dithiolane groups to enhance affinity to the metal surface; all three ligands share a common zwitterion group (made of sulfobetaine) to promote water solubility, as shown in **Figure 1**. The synthetic rationale can also be used to prepare small ligands presenting either a terminal amine or a carboxyl group, which can be used for further modification of the nanocrystals with proteins and dyes using simple coupling chemistries[40]. We further combine this ligand design with a recently devised photoligation strategy to promote the phase transfer of the nanocrystals under borohydride-free conditions[40]. The resulting hydrophilic nanoparticles exhibit excellent colloidal stability over a broad range of conditions, including acidic and basic buffers, high electrolyte concentrations, in the presence of a biogenic thiol molecules (such as glutathione), and storage at room temperature (22–25 °C) and under exposure to white light. The compactness of the ligand design is further demonstrated by conjugating the zwitterion-functionalized QDs to maltose-binding protein (MBP) or the fluorescent mCherry protein expressing terminal polyhistidine tags. This confirms that indeed direct access and coordination of the histidine-tag onto the metal surface of the nanocrystals is achieved. QD-mCherry conjugates prepared through this route have been characterized using fluorescence resonance energy transfer (FRET) interactions, whereas QD-MBP conjugates were characterized using affinity chromatography[40,41]. In fact, metal-histidine conjugation of proteins on QDs can be applied using a variety of proteins expressed with a polyhistidine tag. In addition, verification of the conjugation can be carried out using other analytical tools including biological assays and gel electrophoresis.

Experimental design

Rationale for the ligand design and the use of the photoligation strategy. This protocol introduces a straightforward synthetic route to prepare molecular-scale multicoordinating zwitterion ligands combined with a photoinduced chemical ligation strategy to promote the transfer of hydrophobic QDs to polar and buffer solutions. High-quality CdSe-ZnS QDs that are used in a variety of studies are prepared using pyrolysis of organometallic precursors at high temperature and in coordinating solution according to the schemes that are previously described in several reports[9,42–44]. First, the CdSe core is grown using cadmium and selenium precursors at a temperature of 300–350 °C. Subsequently, the core is overcoated with a few monolayers of ZnS or ZnCdS in the second step, but the procedure is carried out at a slightly lower temperature (120–180 °C) using a mixture of zinc, cadmium and sulfur precursors. Additional details on the quantum dot synthesis are described in previous publications[13,42,43]. As made, these nanocrystals are stabilized with hydrophobic ligands (such as TOP/TOPO and phosphonic acid), resulting in mainly hydrophobic materials. This requires that an effective surface functionalization strategy be developed to promote the transfer of these materials to buffer solutions, while maintaining great colloidal stability, chemical reactivity and, if possible, compact dimensions.

To achieve this goal, we focus on the design and synthesis of a series of LA–based multicoordinating ligands in which the hydrophilic moiety is made of a sulfobetaine-based zwitterion group. As made in their oxidized form, such ligands can easily coordinate onto Au nanoparticles[27]. However, reduction of the LA to DHLA is required to facilitate coordination onto the surface of semiconductor QDs[25,27]. Although chemical reduction of the LA groups using sodium borohydride has been effectively used in previous studies[20,25,26], we have recently found that in situ photochemical ligation of such ligands onto the surface of QDs provides a new strategy that is mild and more effective for promoting the transfer of QD materials to buffer solutions. This ligand design is also motivated by the desire to reduce the overall hydrodynamic diameter of the QDs by reducing the thickness of the hydrophilic coating layer. This requirement is crucial for adapting these nanomaterials to certain sophisticated applications in biology. For example, large size can limit the access of QDs to confined spaces inside the cells and prevent renal clearance[14,45].

Pure dihydrolipoic acid (DHLA) was first used by our group to prepare compact CdSe-ZnS QDs in aqueous medium, but this ligand limits the QD and Au nanoparticle solubility to basic buffer conditions[25]. Subsequent developments by our group and others have expanded the colloidal stability of QDs to a broader range of biological conditions by appending PEG moieties onto the LA[18]. After that development, we showed that insertion of two LA groups onto a single PEG chain provides improved colloidal stability to QDs and AuNPs compared with mono-LA-appended ligands[27]. However, the use of a PEG chain, although effective for expanding the colloidal stability of QDs to acidic pH, tends to increase the hydrodynamic size of the nanocrystals. More recently, LA–appended ligands presenting sulfobetaine moiety (zwitterion, ZW) have been developed to provide hydrophilic nanocrystals[24,28,41,46]; in those studies, the authors have substituted PEG with a small zwitterion segment. These developments have motivated us to design three sets of LA-appended zwitterion ligands and combined them with the above photoligation strategy to prepare compact, colloidally stable and reactive QDs (**Figs. 1** and **2**).

The photoligation strategy, which promotes the photochemical transformation of the LA, allows one to use the oxidized form of the ligand along with a smaller amount of materials during the ligand exchange step, which drastically simplifies the phase transfer procedure. This approach is well adapted to an array of LA-based ligands (LA, LA-PEG, LA-ZW, bis(LA)-ZW)), and, more importantly, it preserves the integrity of several reactive groups with great relevance in biology such as aldehyde and azide; these groups are readily altered during the chemical reduction using borohydride. The photoligation strategy is also ideally suited for zwitterion-modified ligands, owing to the difficulty associated with the preparation and purification of the chemically reduced form of such ligands. After the phase transfer, the QD materials form homogeneous dispersions in water, and their optical and spectroscopic characteristics are maintained. We have previously published two papers in *Nature Protocols* detailing the synthesis of a series of PEG-appended LA ligands (prepared with various terminally reactive groups and different PEG sizes) and their use for the functionalization of QDs and Au nanoparticles alike[21,35]. We have also described the combination of zwitterion-modified LA ligands with UV irradiation to promote the transfer of QDs in a previous report[47]. Here we expand those approaches by detailing the synthesis of higher-order LA-ZW ligands (namely bis(LA)-ZW) and show that when combined with photochemical ligation they yield QDs that exhibit enhanced colloidal stability, are compact in size and compatible with metal-histidine coordination. Additional details about the steps involved in the photoligation and the rationale for its effectiveness can be found in our recent reports[8,41].

Functionalization of the QDs. The synthesis of the LA-ZW ligand involves two steps: *N*,*N*-dimethyl 1,3-propanediamine is first attached onto the LA, followed by reacting with 1,3-propanesultone (**Fig. 1a**; ref. 41). Similarly, to prepare LA-TEG-ZW, LA-TEG-NH_2 is first coupled to 4-(dimethylamino)butyric acid in the presence of DCC (*N*,*N*′-dicyclohexylcarbodiimide)

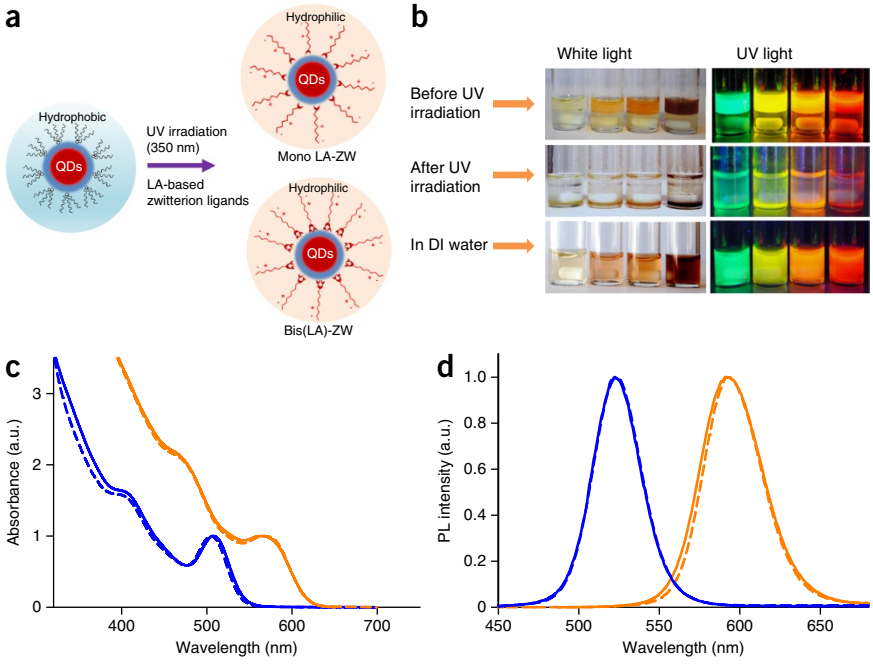

Figure 2 | Photoligation strategy to prepare hydrophilic QDs. (**a**) Schematic representation of the photoligation strategy applied to the hydrophobic QDs (capped with TOP/TOPO, phosphonic acid and alkylamines) with LA-ZW and bis(LA)-ZW. (**b**) Images of a set of QDs of different sizes (with λ_{em}= 540, 574, 585 and 624 nm) transferred from hexane (top layer) to methanol (bottom layer) and finally dispersed in water; the ligand exchange was carried out using LA-ZW. (**c**,**d**) UV-visible absorption spectra, normalized with respect to the first absorption peak (**c**), and photoluminescence spectra, normalized with respect to the peak value (**d**), of two representative sets of QDs. The dotted line represents hydrophobic QDs in hexane and the solid line corresponds to LA-ZW-QDs dispersed in water. a.u., arbitrary units. Adapted from ref. 41 with permission from the American Chemical Society.

and DMAP (4-dimethylaminopyridine), followed by reaction with 1,3-propanesultone (**Fig. 1b**). As the shortest member in the PEG family, LA-TEG-ZW provides more compact nanocrystals while maintaining biocompatibility; DHLA-TEG-capped QDs are not stable in buffer solutions[18]. The third set of zwitterion ligands are appended with two LA groups instead of one; they include bis(LA)-ZW, bis(LA)-NH_2 and bis(LA)-COOH (**Fig. 1c**). The presence of two LA anchoring groups is greatly beneficial for this ligand exchange strategy, as it provides QDs and AuNPs with colloidal stability extending to highly acidic and basic conditions and in the presence of a high concentration of reducing agents[27,40].

We found that the dispersions of QDs photoligated with mono-LA-ZW ligands remain fluorescent and aggregate-free over the pH range from 3 to 13 and in the presence of excess salt and growth medium for several months of storage. Photoligation of the QD with bis(LA)-ZW ligands yields QD dispersions that remain homogeneous for over 1.5 years of storage at 4 °C. Furthermore, homogeneous dispersions of QDs prepared with bis(LA)-ZW can be stored under ambient conditions (room temperature and light exposure) and at nanomolar concentrations for over 3 months, while maintaining high fluorescence emission. In addition to the small hydrodynamic size afforded by the zwitterion ligands, introducing a small molar fraction of bis(LA)-NH_2 and bis(LA)-COOH during the ligand exchange provides QDs with a controlled fraction of reactive surface groups. For this, a small molar amount of amine- or carboxy-terminated ligands is mixed with bis(LA)-ZW during the photoligation procedure. We should note that all the chemical reactions described here are based on simple coupling chemistry (e.g., *N*,*N*′-dicyclohexylcarbodiimide (DCC) or CDI (1,1′-carbonyldiimidazole)), and thus they can be easily scaled up. Finally, although we have used CdSe-ZnS core-shell QDs in our study, the ligands described here can also be applied to other types of nanocrystals made of CdSe, CdS, InAs and InP cores and CdS, ZnS or ZnSeS shells.

Metal-histidine self-assembly of QD-protein conjugates. To show the biological utility of these materials, we self-assemble the QDs photoligated with LA-ZW, LA-TEG-ZW or bis(LA)-ZW with histidine-tagged full-size proteins (MBP-His_8 or MBP-His_7 and mCherry-His_6); this allows us to test the compatibility of the resulting compact QDs with metal-histidine–driven interactions. The conjugation method involves the interactions between the polyhistidine tag appended on the proteins with the Zn-rich QD surfaces. Its effectiveness is limited to the use of small capping ligands (e.g., zwitterion-modified ligands), as large ligands tend to block direct access of the imidazole groups on the histidine tag to the QD surfaces[48]. We should note that QD conjugates prepared via this route can be used in several targeted biological applications, which include visualizing ligand-receptor interactions on surface membranes and intracellular uptake of cargo proteins, and visualizing cancer tissues[24,26,49–51].

Conjugation of proteins onto the QD surface promoted by metal-histidine self-assembly can be examined using a few simple analytical tests. One of them relies on tracking the increase in the QD photoluminescence following conjugation with the number of bound protein per QD; this is suitable for nonfluorescent proteins[25,37]. The photoluminescence intensity reaches a plateau when the surface of the nanocrystal is saturated with bound proteins (i.e., a configuration of near closely packed proteins on the nanoparticle). In general, we observe an increase in the photoluminescence ranging from 0 to 200% for QDs photoligated with bis(LA)-ZW, depending on the molar ratio and QD sample used[40].

Another practical and visual test uses affinity chromatography involving immobilization of the QD-MBP-histidine conjugates onto an amylose gel column, followed by release with soluble maltose. The third test probes FRET interactions within self-assembled QD-mCherry-histidine conjugates. This test also requires close proximity between the QD donor and mCherry acceptor, and it provides a quantitative measurement for the number of proteins per QD conjugate, as well as an idea about the lateral extension of the protein on the QD surface from the experimental FRET efficiency. Finally, we should emphasize that QDs photoligated with these sets of zwitterion ligands combined with the easy-to-implement protein conjugation, especially fluorescent proteins, can be used to develop advanced analytical sensing and imaging tools based on FRET.

Some of the most important advantages of the present approach include not having to rely on chemical reduction of the ligands and the use of very compact and multicoordinating ligands. The latter provides QDs that are small in hydrodynamic size and compatible with metal-histidine coordination. Limitations of the present protocol derive from the fact that the synthesis of zwitterion ligands can be tedious owing to the stringent solubility requirements brought by the nature of the zwitterion groups; zwitterion-containing molecules are often soluble only in water and a few polar solvents. Therefore, during the synthesis process, the solubility of the precursor(s) and product(s) needs to be carefully controlled. In addition, overdrying the intermediate and final products can reduce solubility, and thus it should be avoided.

MATERIALS

REAGENTS

! CAUTION Most of the chemicals used and listed below are hazardous (e.g., toxic, irritant, corrosive, flammable and lachrymator); they must be carefully handled.

- Lipoic acid (LA) or thioctic acid (Sigma-Aldrich)
- Tetraethylene glycol (TEG; Sigma-Aldrich)
- LA-TEG-NH_2 (ref. 52)
- Triethylamine (Et_3N; Sigma-Aldrich)
- Methanesulfonyl chloride (Sigma-Aldrich) **! CAUTION** This highly toxic reagent should be handled in a fume hood.
- *N*,*N*-Dimethyl-1,3-propanediamine (Alfa Aesar) **! CAUTION** This highly toxic and volatile reagent should be handled in a fume hood.
- 4-(Dimethylamino)butyric acid hydrochloride (Sigma-Aldrich)
- 1,3-Propanesultone (Alfa Aesar) **▲ CRITICAL** This reagent is moisture-sensitive. Storage in a desiccator is recommended.
- *N*,*N*′-Dicyclohexylcarbodiimide (DCC; Fluka) **▲ CRITICAL** This reagent is sensitive to moisture. Storage in a desiccator is recommended.
- 4-Dimethylaminopyridine (DMAP; Acros Organics or Sigma-Aldrich)
- Tris(2-aminoethyl)amine (Alfa Aesar)

- Succinic anhydride (Sigma-Aldrich) ▲ **CRITICAL** This reagent is moisture-sensitive. Storage in a desiccator is advised.
- 1,1′-Carbonyldiimidazole (CDI; Sigma-Aldrich)
- Sodium carbonate (Na_2CO_3; Acros Organic)
- Sodium sulfate, anhydrous (Sigma-Aldrich)
- Iodine (Sigma-Aldrich)
- Silica gel (60 Å, 230–400 mesh; Bodman Industries) ! **CAUTION** This should be handled with a proper dust mask, while preparing the column.
- Chloroform ($CHCl_3$)
- Methanol (MeOH)
- Deuterated DMSO (DMSO-d6; Cambridge Isotope Laboratories)
- Deuterated chloroform ($CDCl_3$; Cambridge Isotope Laboratories)
- Phosphoric acid (Sigma-Aldrich)
- Hydrochloric acid (EMD Chemicals)
- Phosphate buffer salts (Sigma-Aldrich)
- Amylose resin (New England BioLabs)
- D-(+)-Maltose monohydrate (Sigma-Aldrich)
- pMal-c2 plasmid (New England BioLabs)
- pBADplasmid (New England BioLabs)
- *Escherichia coli* BL21 cells (Novagen)
- Luria-Bertani broth base (LB; Invitrogen)
- Isopropyl β-D-thiogalactoside (IPTG; Fisher Scientific)
- Nickel affinity gel (Sigma-Aldrich)

EQUIPMENT

! **CAUTION** Exposure to UV light is harmful to the eyes and skin. Appropriate safety procedures should be followed during experiments.

- Round-bottom flasks, one (100 and 250 ml)-, two (250 ml)- and three (250 ml)-necked
- Addition funnels (25 and 50 ml)
- Separatory funnels (250 ml)
- Glass funnels
- Magnetic stirring bars
- Filter paper
- Rotary evaporator
- Thin-layer chromatography (TLC) plates (silica gel matrix with aluminum support; Fisher Scientific)
- Iodine chamber for staining TLC plates
- Syringe filters (0.22 µm) compatible with biological samples
- Centrifugal filtration devices (MWCO 50 kDa, Millipore)
- Disposable plastic columns (5 ml; Fisher Scientific)
- Amicon Ultra-15 centrifugal filter unit with Ultracel-50 membrane (Millipore, MWCO ~50 kDa)
- Centrifuge (IEC Centra CL2 centrifuge, Thermo Scientific)
- Microcentrifuge tubes (1.5 ml; Eppendorf International)
- Quartz cuvettes (Spectrocell)
- Hand-held UV light source (365 nm excitation)
- Photoreactor (Luzchem UV lamp, model LZC-4 V)
- Spectrometer (e.g., Fluorolog-3 from JobinYvon)
- UV-visible spectrophotometer (e.g., UV 2450 model from Shimadzu Scientific)
- NMR spectrometer (e.g., BrukerSpectroSpin 600 MHz spectrometer)

REAGENT SETUP

Protein expression We anticipate that the polyhistidine-driven self-assembly on the above QDs will be applicable to any protein that is engineered to express a terminal polyhistidine-tag (made of ~5–10 amino acids). We tested this conjugation strategy onto our QDs using MBP and the fluorescent mCherry protein. We briefly describe the expression of these two proteins. The pMal-c2 plasmid containing an insert for MBP was engineered to express a sequence of eight histidines (His_8). The sequence encoding MBP, spanning K1 to T366, was modified within the pMal-c2 vector (New England Biolabs) to introduce an 8× histidine tag, with NSSSHHHHHHHHSSGLVPRGSS residues at the C terminus of MBP. The protein was expressed in BL21 cells; LB medium was inoculated 1:100 with saturated culture, grown to an optical density at 600 nm (OD_{600}) of 0.6, and treated with 0.4 mM ITPG. After induction, the culture was harvested for 3 h and then lysed using a microfluidizer in binding buffer (50 mM sodium phosphate, pH 8.0, 300 mM NaCl and 10 mM imidazole). Clarified lysate was first purified on a His-Select nickel affinity gel, and then on an anion exchange HPLC system using a linear gradient from 0 to 1 M NaCl, 20 mM Tris and 2 mM EDTA buffer, pH 7.4. The solution was concentrated using a 10-kDa Centricon membrane filter and stored over the short term at 4 °C or flash-frozen for storage at −80 °C. Similarly, we prepared and tested MBP expressing a terminal seven-histidine (His_7) tag, MBP-His_7. The His_6-mCherry protein was expressed using a pBAD plasmid. Expression was carried out in the same BL21 cells (as those used for MBP), but induction was done using 0.2% arabinose, with a few modifications. For purification and characterization, we followed the same procedure used for the MBP, as done above.

LA-TEG-NH_2 Synthesis of LA-TEG-NH_2 was carried out by following the method detailed in Susumu *et al.*[52]. Additional details are provided in the **Supplementary Methods**.

EQUIPMENT SETUP

NMR For characterization of the ligands by ^1H NMR, the chemical shifts in the ANTICIPATED RESULTS section are reported relative to the tetramethylsilane (TMS) signal ($\delta = 0.00$ p.p.m.) in deuterated solvent(s). All *J*-values are reported in Hertz.

PROCEDURE

Synthesis of LA-*N*,*N*-dimethyl 1,3-propanediamine ● TIMING 1 d

1| In a 250-ml three-necked round-bottom flask, dissolve LA (6 g, ~3×10^{-2} mol) and Et_3N (4.19 ml, ~3×10^{-2} mol) in CH_2Cl_2 (60 ml). Next, mount an addition funnel onto the flask.

2| Cool the reaction mixture to ~0 °C using an ice bath, and then stir it for 30 min under N_2 atmosphere.

3| Add methanesulfonylchloride (2.32 ml, ~3×10^{-2} mol) dropwise using the additional funnel, and then gradually warm up the reaction mixture and leave it stirring for ~5 h.

4| Mix *N*,*N*-dimethyl-1,3-propanediamine (3.05 ml, ~2.4×10^{-2} mol), Et_3N (1.67 ml, ~1.2×10^{-2} mol) and 40 ml of CH_2Cl_2in the mounted addition funnel.

5| Add this solution to the flask dropwise (approximately over 30 min) under nitrogen, and then leave the reaction mixture stirring for 10–12 h.

6| Transfer the reaction mixture to a separation funnel, wash it with water (60 ml, two times), and then wash it with saturated Na_2CO_3 solution (two times).

7| Dry the organic layer over 5–10 g of Na_2SO_4 (or $MgSO_4$) for 20–30 min while stirring, and then filter off Na_2SO_4 through a filter paper.

8| Evaporate the solvent using a rotary evaporator; the compound is stable at all relevant temperatures (from room temperature to 100 °C).
■ **PAUSE POINT** Storage of the product in 10–20 ml of CH_2Cl_2 in a refrigerator (4 °C) is recommended, as overdrying of the compound may result in insolubility in $CHCl_3$ during the next step. The compound is stable for at least 10 months when stored in CH_2Cl_2 solution.

Synthesis of LA-ZW ● TIMING 3 d
9| Load LA-*N*,*N*-dimethyl-1,3-propanediamine (4.0 g, ~1.4×10^{-2} mol) and 60 ml of $CHCl_3$ in a 100-ml one-necked round-bottom flask equipped with a magnetic stir bar.

10| Purge the mixture with nitrogen.

11| In a separate vial, heat the 1,3-propanesultone until melting, and transfer it to a syringe.

12| Add the liquid 1,3-propanesultone (1.4 ml, 1.6×10^{-2} mol) into the reaction mixture, and then leave it stirring at room temperature under N_2 atmosphere for 3 d.
▲ **CRITICAL STEP** The reaction solution becomes turbid when complete transformation to the final LA-ZW takes place.
? TROUBLESHOOTING

13| Evaporate the solvent using a rotary evaporator and dry the product under vacuum. Once it is dry, the product is not soluble in $CHCl_3$.

14| Rinse the crude product with 50–60 ml of $CHCl_3$ (three times), remove the solvent containing impurities using a pipette and dry the product under vacuum.

15| Store the product in a refrigerator under nitrogen atmosphere.

Synthesis of LA-TEG-*N*,*N*-dimethyl aminobutyric acid ● TIMING 1 d
16| Load 4-(dimethylamino)butyric acid hydrochloride (0.33 g, ~0.2×10^{-2} mol), Et_3N (0.41 ml, ~0.3×10^{-2} mol) and 30 ml of $CHCl_3$ into a 250-ml three-necked round-bottom flask (equipped with a stir bar) under ice-cold conditions. Stir the solution until it becomes clear.

17| Add DCC (0.41 g, ~0.2×10^{-2} mol) and DMAP (0.05 g, 0.4×10^{-3} mol) in 20 ml of $CHCl_3$ under ice-cold conditions while stirring under N_2.

18| Add a solution of LA-TEG-NH_2 (0.5 g, 0.13×10^{-2} mol in 20 ml of $CHCl_3$) dropwise through an addition funnel while stirring.

19| Once the addition is complete, let the reaction mixture gradually warm up to room temperature, and leave it stirring for ~9 h (or overnight) under N_2 atmosphere.

20| Filter off the white precipitate through a filter paper, and wash the $CHCl_3$ layer with water (30 ml, two times) and then with saturated Na_2CO_3 solution (30 ml, two times).

21| Dry the $CHCl_3$ layer over 5 g of Na_2SO_4 (20–30 min), and then filter off the Na_2SO_4.

22| Evaporate the solvent using a rotary evaporator and dry the product under vacuum.
■ **PAUSE POINT** Storage of the product dissolved in 10–20 ml of CH_2Cl_2 solution in a refrigerator is recommended, as the dried compound can become insoluble in $CHCl_3$ with time. The compound is stable for at least 10 months.

Synthesis of LA-TEG-ZW ● TIMING 3 d
23| Mix LA-TEG-*N*,*N*-dimethyl aminobutyric acid (0.3 g, ~0.6×10^{-3} mol) and $CHCl_3$ (30 ml) in a 100-ml one-necked round-bottom flask equipped with a stir bar.

24| Purge the reaction flask with nitrogen.

25| Add premelted 1,3-propanesultone (0.06 ml, 0.68 × 10^{-3} mol) to the reaction flask using a syringe, and leave the mixture stirring for 3 d at room temperature.

26| Evaporate the solvent using a rotary evaporator, and dry the product under vacuum. Rinse the crude product with ethyl acetate (60 ml, three times), pipette out the solvent containing impurities and dry the product under vacuum.

27| Store the product in a refrigerator under nitrogen atmosphere.

Synthesis of bis(LA)-NH_2 ● TIMING 2 d

28| Dissolve tris(2-aminoethyl)amine (1.5 ml, ~1.0 × 10^{-2} mol) in $CHCl_3$ (40 ml) using a 250-ml one- or two-necked round-bottom flask equipped with a stir bar and an addition funnel.

29| Separately, add LA (5.0 g, ~2.43 × 10^{-2} mol) and CDI (4.3 g, ~2.65 × 10^{-2} mol) in a 250-ml three-necked round-bottom flask. Purge the flask with nitrogen and add $CHCl_3$ (40 ml) via a syringe. Stir the reaction solution for 2 h at room temperature and under nitrogen atmosphere. Add this solution dropwise (via the addition funnel) to the flask containing the solution of tris(2-aminoethyl)amine. Next, leave the reaction stirring for 2 d under nitrogen atmosphere.
▲ **CRITICAL STEP** The addition of the CDI-activated LA to the vial containing tris(2-aminoethyl)amine must be carried out slowly to guarantee that indeed only two of the amines are modified with LA. This also decreases the byproducts such as mono- and tris-modified compounds.

30| Transfer the reaction mixture to a separating funnel. Wash it with water (30 ml, two times) and then with saturated Na_2CO_3 (30 ml, three times).

31| Dry the $CHCl_3$ layer over 5–10 g of Na_2SO_4. Filter out the Na_2SO_4 through a filter paper and evaporate the solvent using a rotary evaporator.

32| Purify the crude product on a silica gel column using 20:1 (vol/vol) $CHCl_3$:MeOH mixture as the eluent; this removes the organic impurities. Owing to their high polarity, the compound shows a baseline migration spot on a TLC plate (i.e., R_f ~0 is measured using 10:1 (vol/vol) $CHCl_3$:MeOH mixture as eluent). The product is then eluted off the column using a 5:1 (vol/vol) $CHCl_3$:MeOH mixture.

33| Evaporate the solvent and concentrate the product using a rotary evaporator.
■ **PAUSE POINT** Storage of the product dissolved in 10–20 ml of $CHCl_3$ in a refrigerator is recommended. A thoroughly dried compound may become insoluble in $CHCl_3$ with time. The compound is stable for at least 10 months.

Synthesis of bis(LA)-COOH ● TIMING 1 d

34| Load bis(LA)-NH_2 (~0.52 g, 0.93 × 10^{-3} mol), $CHCl_3$ (40 ml), succinic anhydride (1.92 g, 0.19 × 10^{-2} mol) and Et_3N (0.27 ml, 0.19 × 10^{-2} mol) in a 100-ml round-bottom flask equipped with a magnetic stir bar. Purge the flask with nitrogen and leave the reaction mixture stirring overnight.

35| Wash the reaction mixture with water (30 ml, two times). Dry the organic layer over Na_2SO_4 (~5 g), filter it through a filter paper and evaporate the solvent.

36| Purify the crude product by chromatography on a silica column using a mixture of 6:1 (vol/vol) $CHCl_3$:MeOH as the eluent. Elute the material under gravity and collect 50–100-ml fractions. The compound has a high polarity, and it shows a near baseline spot on a TLC plate (i.e., R_f ~0.1 is measured using 10:1 (vol/vol) $CHCl_3$:MeOH mixture as eluent). Confirm the purity of this product by ^1H NMR spectroscopy.

37| Evaporate the solvent using a rotary evaporator.
■ **PAUSE POINT** Storage of the product in 10–20 ml of $CHCl_3$ in a refrigerator is recommended. The compound is stable for at least 10 months.

Synthesis of bis(LA)-*N*,*N*-dimethyl alkyl amide ● TIMING 2 d

38| Load *N*,*N*-dimethylaminobutyric acid hydrochloride (0.72 g, 0.43 × 10^{-2} mol), Et_3N (0.66 ml, 0.47 × 10^{-2} mol) and $CHCl_3$ (30 ml) into a two-necked 250-ml round-bottom flask equipped with a stir bar and an addition funnel. Stir the mixture until the compounds are completely dissolved (~30 min).

39| Add DCC (0.59 g, 0.29 × 10^{-2} mol) and a catalytic amount of DMAP (0.07 g, 0.57 × 10^{-3} mol) in $CHCl_3$ (20 ml) under ice-cold conditions, and then stir the reaction mixture for 30 min.

40| Load bis(LA)-NH_2 (1.5 g, 0.29 × 10^{-2} mol) and $CHCl_3$ (40 ml) onto the addition funnel, and then slowly add the contents (dropwise) to the above reaction mixture. Next, leave it stirring at room temperature under N_2 atmosphere for 2 d.

41| Filter out the white precipitate and wash the $CHCl_3$ solution with saturated Na_2CO_3 solution (30 ml, two times).

42| Evaporate the $CHCl_3$ using a rotary evaporator and chromatograph the residue on a silica gel column. The product is collected using 6:1 (vol/vol) $CHCl_3$:MeOH as the eluent. The compound shows a baseline migration on the TLC plate owing to the high polarity (i.e., R_f ~0 is measured using 10:1 (vol/vol) $CHCl_3$:MeOH mixture as eluent).

Synthesis of bis(LA)-ZW ● TIMING 3 d

43| Dissolve bis(LA)-*N*,*N*-dimethyl alkyl amide (1.0 g, 0.16 × 10^{-2} mol) in 20 ml of $CHCl_3$.

44| Add 1,3-propanesultone (0.17 ml, 0.19 × 10^{-2} mol) via a syringe under N_2 and leave the mixture stirring at room temperature for 3 d.

45| Concentrate the solution by partially evaporating one-half to two-third of the $CHCl_3$ from the solution.
■ **PAUSE POINT** Storage of the product dissolved in 10–20 ml of $CHCl_3$ in a refrigerator (4 °C) is recommended. The solution can be stored for more than 1 year.

Photoligation of LA-ZW ligands onto hydrophobic QDs and phase transfer ● TIMING ~2 h

46| Transfer 200 µl of TOP/TOPO-QDs in hexane/toluene mixture (~7 µM stock solution) to a scintillation vial.

47| Add ethanol and centrifuge the solution (1,900*g* for 15 min at room temperature) to precipitate out the TOP/TOPO-QDs. This produces a colored pellet.

48| Discard the supernatant and re-disperse the QD pellet in 0.5 ml of hexane.

49| In a separate scintillation vial, add LA-ZW ligand (35 mg) and 500 µl of MeOH, and slightly heat the solution (~50–60 °C) while stirring until the ligand is completely dissolved and the solution becomes clear.
▲ **CRITICAL STEP** The solubility of the zwitterion ligand in MeOH is not immediate. A slight heating while stirring is required. This readily produces a homogeneous yellowish solution.
▲ **CRITICAL STEP** The amount of ligand required varies from one zwitterion ligand to another depending on their molecular weight and structure. For instance, we used 53 mg of LA-TEG-ZW and 44 mg of bis(LA)-ZW. A smaller molar amount of ligands with respect to QDs can also be used for bis(LA)-ZW-QDs.

50| Add catalytic amount (~10 mM) of tetramethyl ammonium hydroxide (TMAH) base to the MeOH solution containing the zwitterion ligands.

51| Mix the ligand solution in MeOH and the hexane solution of TOP/TOPO-QDs in a vial equipped with a magnetic stir bar.

52| Seal the scintillation vial with a septum and switch the atmosphere to nitrogen by applying two or three rounds of mild vacuum, followed by purging with nitrogen. Note that the procedure can be carried out without purging with nitrogen, as shown in our recent work[53].

53| Place the vial inside the UV reactor and irradiate for 30–40 min while stirring. This produces aggregates of QDs throughout the sample.
▲ **CRITICAL STEP** Irradiation of the sample in the UV range 300 < λ < 400 nm is a prerequisite for an effective and successful ligand exchange and phase transfer of the QDs. In the present experiments, we have used an irradiation signal at 350 nm with a power of 4.5 mW cm^{-2}. Under these conditions, the time necessary for complete cap exchange and phase transfer may slightly vary between 20 and 40 min from one sample to another, depending on the amount of TOP/TOPO-QDs used. Sample irradiation in the 'visible' region leads to incomplete ligand exchange even if a longer irradiation time is used.
▲ **CRITICAL STEP** The photoirradiation must be carried out using a two-phase solution, because of the stringent and vastly different solubility requirements for the native QDs and the zwitterion ligands.
? TROUBLESHOOTING

54| Remove the solvents containing solubilized free hydrophobic ligands (e.g., TOP and TOPO) and excess free zwitterion ligands using a pipette.

55| Wash the QD aggregates with MeOH (two times) followed by centrifugation; discard the solvents using a pipette after each wash.
? TROUBLESHOOTING

56| Dry the QDs for 1–2 min under vacuum.
▲ **CRITICAL STEP** Gentle drying (e.g., by applying mild vacuum using a Schlenk line for 1–2 min) is recommended.

57| Add 3 ml of deionized (DI) water to disperse the nanocrystals.
▲ **CRITICAL STEP** Addition of a small amount of TMAH to the dispersion and subsequent sonication (~2–5 min) after ligand exchange accelerates the dispersion of QDs photoligated with bis(LA)-ZW in water. The amount of TMAH (a few milligrams) can be adjusted until homogeneous dispersion of QDs in water is observed after sonication.

58| Pass the solution through a 0.45-μm syringe filter (e.g., a Millex-LCR filter from Millipore).

59| Transfer the filtrate to an Amicon Ultra centrifugal membrane filtration device and add more DI water until the device is full (~15 ml total).

60| Centrifuge the sample (~1,900–2,000*g*, 5–10 min) at room temperature and discard the filtered solution.

61| Repeat the procedure two times to effectively remove all free ligands from the dispersion.

62| Transfer the QD dispersions in a vial and store it in refrigerator until further use.
■ **PAUSE POINT** Storage of the QD dispersions at 4 °C in a refrigerator is advised. This extends the shelf-life of the samples to 12 months and longer. The characterization of QDs can be carried out by measuring UV-visible and photoluminescence spectra to examine the optical properties of QDs, and red shift of emission peak will be observed if QD samples aggregate.

Self-assembly of histidine-tagged proteins onto zwitterion-capped QDs

63| In options A and B, we provide two example procedures for conjugating the quantum dots with proteins. Small adjustments may be needed when using different histidine-tagged proteins, but the overall steps required and buffers used are similar. Follow the steps in option A if your protein is similar to MBP in that the binding affinity to amylose will allow the sample analysis of sufficient MBP-QD binding via amylose gel assay. Option B is different, because the fluorescent protein mCherry is used. Here, the FRET data are collected for a varying number of mCherry (fluorescent protein) per QD in solution phase and the unbound proteins do not interfere with the energy transfer interactions and ensued quenching. We limit our description to QDs photoligated with bis(LA)-ZW ligands and describe the procedure for preparing conjugates with a varying number of proteins per QD conjugate (i.e., conjugate valence). The metal-histidine conjugation with MBP and mCherry can be easily applied to QDs photoligated with mono LA-ZW[41].

(A) Self-assembly of MBP-histidine onto zwitterion-capped QDs ● TIMING 45 min

(i) Place 8.2 μl of MBP-His_8 (537 μM stock solution) and 90–100 μl of PBS (pH 7.5-8.0) in a microcentrifuge tube.

(ii) In a separate microcentrifuge tube, add 50 μl of ZW-capped QDs stock dispersion (7.3 μM) in PBS buffer (pH 7.5–8.0) to a total volume of 200 μl; these include LA-ZW-QDs, LA-TEG-ZW-QDs or bis(LA)-ZW-QDs.

(iii) Add MBP-His_8 solution to the tube containing the dispersion of QDs, gently mix using micropipette and incubate the sample at ~4 °C for 30–45 min. The amount of protein solution added depends on the targeted molar ratio of MBP-to-QD. An adjustable amount of buffer is also added to reach the desired molar concentration of the QD-protein conjugates in the medium. The conjugates can be used as for the targeted biological assay of choice. Further verification of the conjugate formation can be carried out using affinity chromatography, as described below (Step 63A(iv–vii)).

(iv) Load 1.52 ml of amylose stock gel onto a 10-ml-capacity column and rinse with 10 ml of PBS buffer, pH 7.5.

(v) Load the solution of QD-MBP conjugates onto the column and allow the sample to equilibrate, which produces a fluorescent layer of QD conjugates immobilized on the top of the column.
? TROUBLESHOOTING

(vi) Wash the column with PBS buffer, pH 7.5 (four times, 5 ml each). The QD-MBP conjugates should stay bound on top of the column.
? TROUBLESHOOTING

(vii) Add 5 ml of a 20 mM solution of D-(+)-maltose to the column. This will immediately elute the conjugates, which can be collected in a microcentrifuge tube.

? TROUBLESHOOTING

(B) Self-assembly of mCherry-histidine protein onto zwitterion-capped QDs ● TIMING 45 min

(i) Place 30-µl aliquots of bis(LA)-ZW-QDs stock solution (~3.23 µM) and 70 µl of 10 mM PBS buffer (pH 7.5–8.0) in microcentrifuge tubes to bring the total volume in each sample to 100 µl.

(ii) In separate microcentrifuge tubes, mix varying amounts of His_6-appended mCherry (11.4 µM stock solution) with PBS buffer, adjust the amount of the buffer added to maintain the total volume of 300 µl for each solution, while varying the molar ratio of QD:mCherry from 1:3 to 1:15.

(iii) In a microcentrifuge tube, add the QD dispersion and mCherry solution. Gently mix and incubate all the samples at 4 °C for ~45 min. This should produce dispersions of QD-mCherry conjugates at the desired valences, as indicated above.

▲ CRITICAL STEP When metal-histidine self-assembly is used to form the QD-protein conjugates, a marked enhancement in the photoluminescence emission of the QDs is measured, regardless of whether the protein is fluorescent or not. In addition, such enhancement depends on the valence. This enhancement should be taken into account in the FRET data analysis. This can be done, for example, by assembling a reference plot of photoluminescence versus valence using a nonfluorescent histidine-appended protein (e.g., MBP-histidine)[25,37].

■ PAUSE POINT The QD-protein conjugates (e.g., QD-MBP and QD-mCherry, in this case) are best used when fresh. They can be stored in a refrigerator at 4 °C. However, the biological activity of the conjugates may not be preserved if they are stored over an extended period of time (>1 week), owing to the limited shelf-life of proteins. These tend to denature with time; they are often stored at –80 °C.

? TROUBLESHOOTING

Step 12

If the concentration of sultone is too low, the reaction mixture does not become turbid even after 3 d. Add a small amount of sultone and leave the reaction to proceed for several hours to achieve complete transformation to the zwitterion form of the ligand. The reaction mixture will eventually turn turbid.

Step 53

If the QDs are not completely precipitated out during photoirradiation, the ligand exchange process is incomplete. Reduce the amount of QDs used and/or increase the amount of ligands and the time of irradiation.

Step 55

Sometimes a partial precipitation of the LA-ZW-QDs after addition of MeOH occurs. This may be caused by remaining excess TMAH used in Step 50. Add a mixture of MeOH, $CHCl_3$ and hexane at volume ratio of 1:1:10 to precipitate the QDs, followed by centrifugation at a speed of ~1,900–2,000*g* at room temperature for 6 min. Decant the solvent and slightly dry the sample under vacuum. The QD pellet will readily disperse in DI water.

Step 63A(v,vi)

If only partial binding of the conjugates to the amylose column occurs, the amount of gel materials loaded onto the column is too low to allow complete immobilization of the QD-MBP-histidine conjugates. Increase the volume of gel materials and repeat the experiment.

Step 63A(vii)

If only partial elution of the QD-MBP conjugates takes place, the conjugate concentration is too high for full elution with the amount of added maltose. Increase the volume of maltose solution added to the column.

● TIMING

Steps 1–8, synthesis of LA-*N*,*N*-dimethyl 1,3-propanediamine: 1 d
Steps 9–15, synthesis of LA-ZW: 3 d
Steps 16–22, synthesis of LA-TEG-*N*,*N*-dimethyl aminobutyric acid: 1 d
Steps 23–27, synthesis of LA-TEG-ZW: 3 d
Steps 28–33, synthesis of bis(LA)-NH_2: 2 d
Steps 34–37, synthesis of bis(LA)-COOH: 1 d
Steps 38–42, synthesis of bis(LA)-*N*,*N*-dimethyl alkyl amide: 2 d
Steps 43–45, synthesis of bis(LA)-ZW: 3 d

Steps 46–62, cap exchange of QDs: ~2 h
Step 63A, self-assembly of QD-MBP-histidine conjugates: 45 min
Step 63B, self-assembly of QD-mCherry-histidine conjugates: 45 min

ANTICIPATED RESULTS

In the following section, we provide characterization of the quantum dots prepared using this procedure. The QDs photoligated with the zwitterion ligands are characterized using UV-visible absorption and fluorescence spectroscopy, and conjugation of MBP-$(His)_n$ and mCherry-$(His)_n$ onto the zwitterion-QDs is verified using affinity chromatography and fluorescence spectroscopy. We also show results from tests of the colloidal stability under different pH and ambient storage conditions for two sets of QDs, one photoligated with LA-ZW and the other photoligated with bis(LA)-ZW. The ligands prepared in Steps 1–45 should be characterized using ^{1}H NMR, electrospray ionization mass spectrometry (ESI-MS) and Fourier transform infrared (FT-IR) spectroscopy, and the analytical data for these compounds are provided at the end of this section.

Characterization of the hydrophilic QDs photoligated with LA-ZW ligands

Optical characterization. Figure 2b shows a representative example of phase transfer with LA-ZW ligands using UV photoirradiation (and two-phase configuration) applied to several sets of TOPO/TOPO-QDs emitting over the spectral region spanning from green to red. Shown are images of vials containing the QD materials under white light exposure and UV excitation. Initially, the hydrophobic dots are dispersed in the top hexane layer, whereas the ligands are limited to the bottom MeOH layer. This is further confirmed by the fluorescence images shown on the right where the QD color-specific emission is observed only in the top layer. After UV irradiation, ligand exchange of the nanocrystals with the LA-zwitterion takes place. A macroscopic precipitation of the QDs builds up in the vial, indicating that photoligation with the zwitterion ligands drastically alters the QD solubility: the zwitterion-QDs are not soluble in either hexane or MeOH. After decanting the solvents, the QDs are readily dispersible in DI water, as indicated by the clear, homogeneous dispersions shown in **Figure 2b**. The absorption and emission spectra of all five sets of QDs after transfer to DI water are essentially identical to those collected for the native TOP/TOPO-QDs in toluene, indicating that photoligation does not alter the spectroscopic properties of the nanocrystals; spectra of two representative dispersions are shown in **Figure 2c**,**d**. Nonetheless, phase transfer to water is accompanied by a loss in the overall photoluminescence in comparison with the native hydrophobic QDs; the photoluminescence quantum yield of the water-soluble nanocrystals decreases to 0.5–0.7 of the values measured for the native TOP/TOPO-QDs. For example, if the starting QDs have a photoluminescence quantum yield of 70%, that yield decreases to 35–40% for dispersions in water in a routine experiment.

Colloidal stability. The dispersions of QDs photoligated with the zwitterion ligands exhibit excellent colloidal stability over a broad range of conditions. These include acidic and basic buffers, in the presence of excess electrolytes and to added growth medium. For example, CdSe-ZnS QDs photoligated with LA-ZW and LA-TEG-ZW stay homogeneously dispersed in phosphate buffers over the pH range from pH 3 to 13 and in 50% and 100% RPMI cell growth medium for at least 3 months[40]. Higher coordination ligands (i.e., bis(LA)-ZW) further enhance the colloidal stability of the QDs in buffer solutions. **Figure 3a** shows that dispersions of QDs photoligated with bis(LA)-ZW in phosphate buffers are stable over the pH range of pH 2–14 and in the presence of 1M and 2 M NaCl for at least 18 months of storage at 4 °C.

Additional stability tests were carried out using bis(LA)-ZW-QDs at very low concentrations at room temperature and under light exposure. **Figure 3b** shows that highly dilute dispersions of QDs (at 50 and 100 nM) photoligated with bis(LA)-ZW stay homogeneous and fluorescent for up to 12 weeks, albeit with a slight loss in the photoluminescence signal measured for these dispersions after 3 months. In comparison, a substantial loss in the emission is observed for 50 nM

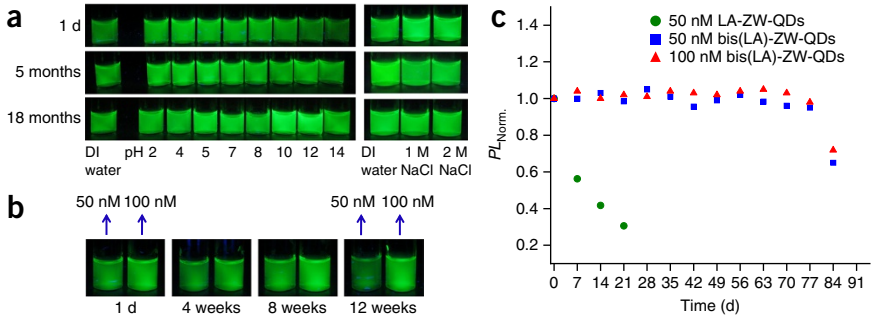

Figure 3 | Stability test of QDs photoligated with bis(LA)-ZW. (**a**) Fluorescence images of bis(LA)-ZW-QD dispersions (λ_{em}=540 nm, 0.5 μM) in phosphate buffer at different pH buffers and in the presence of NaCl (1 and 2 M). Control samples in DI water are also shown; the QD samples have been stored at 4 °C. (**b**) Fluorescence images of dispersions of bis(LA)-ZW-QDs with the indicated molar concentrations, after storage at room temperature and under daylight exposure. (**c**) Plot of photoluminescence (*PL*) intensity versus storage time for dispersions of bis(LA)-ZW-QDs and LA-ZW-QDs with the indicated molar concentrations (**b**). The signal was normalized to the value at day 1. Adapted from ref. 40 with permission from the American Chemical Society.

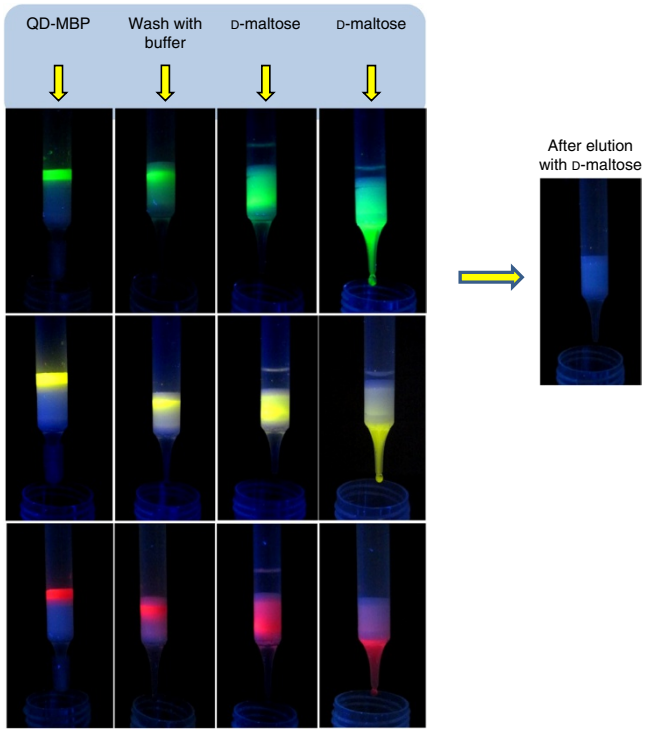

Figure 4 | Affinity chromatography assay applied to the QD-MBP-His_8 assemblies: binding onto the amylose column and release by soluble maltose. When loaded onto an amylose-filled column, the conjugates tightly bind onto the amylose gel and stay bound even after several washes with buffer. They are then readily released by the addition of 1–2 ml of 20 mM maltose solution. Three-color QDs photoligated with LA-ZW ligand are shown: green emitting (λ_{em} = 540 nm), yellow emitting (λ_{em} = 574 nm) and red emitting (λ_{em} = 624 nm, right). Similar results are collected for QDs photoligated with bis(LA)-ZW ligands and self-assembled with either MBP-His_7 or MBP-His_8. Adapted from ref. 41 with permission from the American Chemical Society.

LA-ZW-QDs after 1 week of exposure to daylight under room temperature (**Fig. 3c**). This remarkable enhancement in the colloidal stability is attributed to the higher coordination of the ligands onto QDs photoligated with bis(LA)-ZW. This result is greatly promising for QD use in biological applications in which low concentrations of fluorescent labels are required (e.g., single-molecule tracking and sensing).

Characterization of the QD-MBP conjugates using an affinity chromatography assay

One major advantage of small-molecular-weight zwitterion ligands is providing QDs with very thin hydrophilic coating. Such a thin coating permits direct access of the imidazoles in proteins expressed with a terminal polyhistidine to the QD surface, thus facilitating conjugation with polyhistidine-appended proteins through metal affinity–driven interactions[48,54]. This conjugation route was initially applied to couple DHLA-capped QDs to proteins and peptides[25]. To demonstrate that the present ligand design indeed yields compact nanocrystals, we applied this conjugation strategy to self-assemble QDs photoligated with LA-ZW and bis(LA)-ZW with polyhistidine-tagged MBP (MBP-His_8). The conjugation was confirmed using simple assay based on amylose affinity chromatography[25]. Such test relies on the competition between binding of MBP to an amylose gel and its substrate maltose. As shown in **Figure 4**, when a dispersion of QD-MBP conjugates is loaded onto the amylose column, the presence of the protein in the conjugate promotes binding to amylose, resulting in a clear delineated band on top of the column, which can be visualized using a hand-held UV lamp; the color of the band depends on the photoluminescence of the nanocrystals used. The conjugates stay bound to the column even after several washes with buffers. Addition of 1–2 ml of 10–20 mM D-maltose solution to the column rapidly releases the QD-MBP conjugates, which can be collected in a vial/tube for further use, as shown in **Figure 4**. This behavior unequivocally proves that MBP-His_8 proteins have been self-assembled onto the ZW-capped QDs and that the conjugates maintain the protein biological activity. The latter also proves that the protein orientation in the conjugates is maintained. This assay format has been applied to three sets of zwitterion-modified ligands and using QDs of different sizes[41].

Characterization of the QD-mCherry conjugates using FRET interactions

Conjugation of the zwitterion-QDs to polyhistidine-tagged proteins was further confirmed using a slightly different test: measuring the quenching of QD (donor) photoemission owing to FRET interactions with histidine-tagged mCherry fluorescent proteins. This test allows one to further quantify the number of bound protein per QD after self-assembly. Increasing molar amounts of mCherry-His_6 were mixed with a given concentration of QDs (emitting at 540 nm) in buffer solution. They correspond to protein-to-QD molar ratios between 3 and 15. The concentration of mCherry in the solution was estimated using the extinction coefficient of mCherry (66,314 M^{-1} cm^{-1} at λ = 586 nm), whereas that of the QDs was extracted using the value 8.37×10^5 M^{-1} cm^{-1} at λ = 350 nm. After incubation for 20–30 min to allow for conjugate self-assembly, UV-visible absorption and fluorescence data were collected. The absorption data shown in **Figure 5** indicate that there is an increasing contribution to the measured spectra at 586 nm, commensurate with the amount of added protein to the dispersion, which is attributed to the contribution of mCherry absorption. The composite photoluminescence spectra in **Figure 5c** show that when the dispersions are excited at 400 nm (which coincides with the absorption valley of the protein) there is a progressive decrease in the QD emission concomitant with an increase in the contribution from mCherry when the molar concentration of the protein is increased. Conversely, only a very small (i.e., negligible) photoluminescence signal is collected from the mCherry control solution. The absorption and fluorescence data confirm that conjugate formation has taken place.

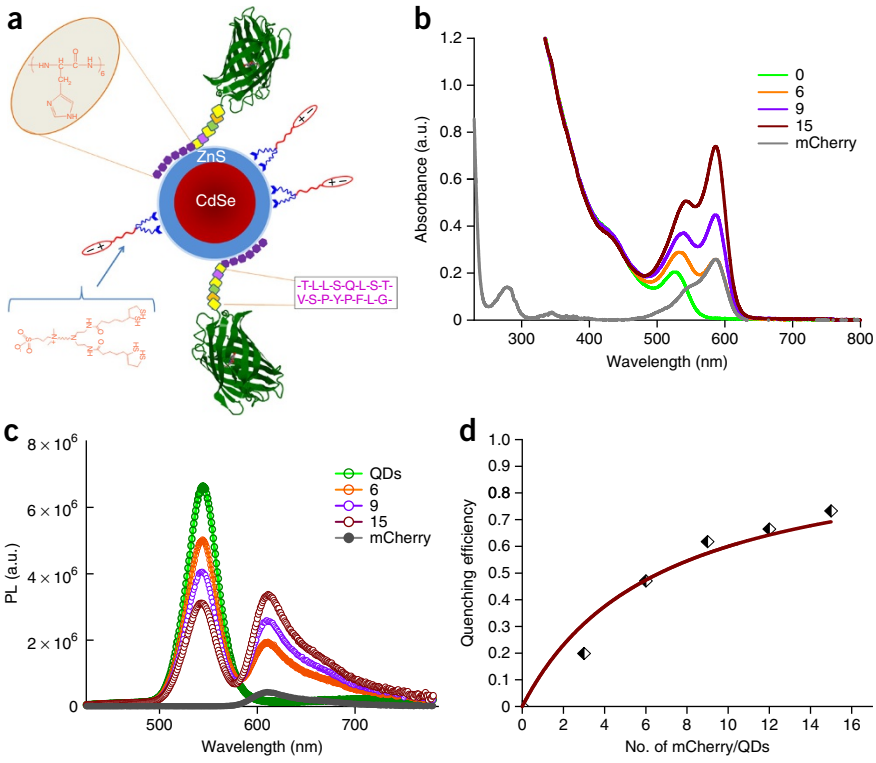

Figure 5 | Protein conjugation of QDs driven by metal-histidine coordination. (**a**) Schematic representation of a self-assembled QD-mCherry conjugate detailing the structure of the different components; a CdSe-ZnS QD photoligated with bis(LA)-ZW ligands is shown. (**b**,**c**) Representative UV-visible composite absorption (**b**) and photoluminescence (PL) spectra (**c**) collected from dispersions of QDs self-assembled with mCherry at different molar ratios of 1:6, 1:9 and 1:15, along with the control samples of QDs and mCherry. The absorption spectra of the conjugates were normalized with respect to the value at 350 nm. The mCherry control spectrum was collected from a solution with the equivalent mCherry concentration of 1:6 above. (**d**) Plot of FRET efficiency versus number of mCherry per QD conjugate. The energy transfer efficiency is extracted from steady-state spectra shown in **c**. a.u., arbitrary units. Adapted from ref. 40 with permission from the American Chemical Society.

Furthermore, the fluorescence data in **Figure 5d** confirm that the strength of energy transfer interactions between the QD and mCherry tracks the conjugate valence anticipated from the molar amounts of added reagents. The QD photoluminescence (or FRET) quenching efficiency is calculated from the fluorescence data using the formula

$$E_n = \frac{F_D - F_{DA}}{F_D} \quad (1)$$

where F_{DA} is the fluorescence intensity of the QD (donor) measured in the presence of mCherry protein (i.e., QD-mCherry conjugates) and F_D is the fluorescence intensity of the QD control[55]. We should note that the control dispersion was actually made of QDs conjugated to an equivalent number of MBP-His_7, to account for the commonly measured enhancement in the QD emission following conjugation to a variety of polyhistidine-appended proteins[25,37].

An expression for the FRET efficiency, E_n, can be extracted for this system using the Förster dipole-dipole formalism and assuming a centro-symmetric configuration for the conjugates (where all the proteins are arrayed around the QD at a fixed separation distance), to correlate the measured efficiency with the center-to-center separation distance, r, and the valence, n:

$$E_n = \frac{nR_0^6}{nR_0^6 + r^6} \quad (2)$$

R_0 is the Förster radius corresponding to $E_{n=1} = 0.5$, given by:

$$R_0 = 9.78 \times 10^3 (n_D^{-4} \times \kappa_p^2 \times Q_D \times I)^{1/6} \quad (3)$$

R_0 (expressed in Å) depends on the photoluminescence quantum yield of the donor, Q_D, the refractive index of the medium, n_D, the dipole orientation parameter, κ_p^2, and the spectral overlap integral, I. A value of $\kappa_p^2 = 2/3$ applies our present configuration[56]. I is extracted from integration (over all wavelengths) of the spectral overlap function, $J(\lambda) = PL_{D\text{-}corr}(\lambda) \times \lambda^4 \times \varepsilon_A$, where PL_D and ε_A designate the normalized fluorescence spectrum of the donor and the extinction coefficient spectrum of the acceptor, respectively. By applying the experimental conditions for our system (a QD radius of ~32 Å (refs. 12,57), a distance between QD-surface and the location of the fluorophore within the mCherry beta barrel of ~28 Å extracted from the protein data bank, PDB)[58], we estimate that the r value is ~ 60 Å. The experimental

data on the quenching efficiency shown in **Figure 5d** are fitted to equation 3 using the above parameters. A good agreement between data and fit is observed. This further confirms that metal affinity–driven self-assembly between these zwitterion-capped QDs and polyhistidine-appended protein is highly efficient and preserves the protein orientation on the QD surfaces. Such findings are in full agreement with previous results on the self-assembly of QDs capped with DHLA and other dye-labeled proteins[56,59].

The optical data, collected from the QD-mCherry system, along with the affinity chromatography test, collected from the QD-MBP-histidine system, clearly prove that the use of LA-ZW ligands combined with the photoligation strategy provide nanocrystals that are colloidally stable and have thin hydrophilic coating, thus allowing easy implementation of the QD-protein conjugation–based metal-histidine self-assembly. Compact QDs capped with zwitterion should exhibit fewer nonspecific interactions than other hydrophilic moieties, and they will be ideally suited for biological applications. These applications include sensor design based on fluorescence detection and/or energy transfer as transduction mechanisms. They also are greatly promising for use in cellular and tissue imaging, as well as in single-protein tracking[5,45,60,61].

Analytical data for the ligands (^{1}H NMR, ESI-MS and FT-IR spectroscopy)

LA-*N*,*N*-dimethyl 1,3-propanediamine

^{1}H NMR (600 MHz, DMSO-d6): δ (p.p.m.) 6.69 (s, 1H), 3.543.59 (m, 1H), 3.323.34 (m, 2 H), 3.093.20 (m, 2H), 2.432.48 (m, 1H), 2.37 (t, 2H, J = 6 Hz), 2.23 (s, 6H), 2.15 (t, 2H, J = 6 Hz), 1.881.93 (m, 1H), 1.671.74 (m, 1H), 1.521.61 (m, 5H), 1.411.52 (m, 2H).

ESI-MS (m/z) calculated for $C_{13}H_{26}N_2OS_2$ $(M)^+$ 290.5; found 290.5.

The reaction yield is ~70%.

LA-ZW

^{1}H NMR (600 MHz, D_2O): δ (p.p.m.) 3.683.72 (m, 1H), 3.453.48 (m, 2H), 3.323.36 (m, 2H), 3.283.30 (m, 2H), 3.163.25 (m, 2H), 3.11 (s, 6H), 2.97 (t, 2H, J = 6 Hz), 2.462.50 (m, 1H), 2.26 (t, 2H, J = 9 Hz), 2.182.22 (m, 2H), 1.962.03 (m, 2H), 1.731.79 (m, 1H), 1.581.67 (m, 4H), 1.391.44 (m, 2H).

ESI-MS (m/z) calculated for $C_{16}H_{32}N_2O_4S_3$ $(M + H)^+$ 413.2; found 413.2.

The reaction yield is ~90%.

LA-TEG-*N*,*N*-dimethyl aminobutyric acid

^{1}H NMR (600 MHz, $CDCl_3$): δ (p.p.m.) 6.84 (s, 1H), 6.33 (s, 1H), 3.423.64 (m, 17H), 3.083.18 (m, 2H), 2.422.47 (m, 1H), 2.32 (t, 2H, J = 9 Hz), 2.24 (t, 2H, J = 9 Hz), 2.22 (s, 6H), 2.18 (t, 2H, J = 9 Hz), 1.861.92 (m, 1H), 1.771.82 (m, 2H), 1.611.72 (m, 4H), 1.41.49 (m, 2H).

ESI-MS (m/z) calculated for $C_{22}H_{43}N_3O_5S_2$ $(M + H)^+$ 494.7; found 494.7.

The reaction yield is ~60%.

LA-TEG-ZW

^{1}H NMR (600 MHz, D_2O): δ (p.p.m.) 3.593.68 (m, 15H), 3.453.48 (m, 2H), 3.363.39 (m, 4H), 3.313.36 (m, 2H), 3.163.25 (m, 2H), 3.1 (s, 6H), 2.96 (t, 2H, J = 6 Hz), 2.622.66 (m, 2H), 2.472.5 (m, 1H), 2.36 (t, 2H, J = 6 Hz), 2.25 (t, 2H, J = 6 Hz), 2.192.22 (m, 2H), 2.052.09 (m, 2H), 1.961.99 (m, 1H), 1.711.77 (m, 1H), 1.571.66 (m, 3H), 1.381.43 (m, 2H).

ESI-MS (m/z) calculated for $C_{25}H_{49}N_3O_8S_3$ $(M + H)^+$ 616.3; found 616.3.

The reaction yield is ~90%.

bis(LA)-NH_2

^{1}H NMR (600 MHz, DMSO-d_6): δ 7.80 (t, 2H, J = 5.5 Hz), 3.62–3.59 (m, 2H), 3.22–3.16 (m, 2H), 3.15–3.10 (m, 2H), 3.10–3.05 (m, 2H), 2.53–2.49 (m, 2H), 2.47–2.37 (m, 7H), 2.12–2.05 (t, 4H, J = 7.4 Hz),1.91–1.82 (m, 2H), 1.88–1.85 (m, 2H), 1.58–1.48 (m, 6H), 1.4–1.31 (m, 4H).

ESI-MS (m/z) calculated for $C_{22}H_{42}N_2O_2S_4$ $(M+H)^+$ 523.3; found 523.2.

The reaction yield is ~35%.

bis(LA)-COOH

^{1}H NMR (600 MHz, DMSO-d_6): δ 7.81 (t, 1H, J = 5.2 Hz), δ 7.74 (t, 2H, J = 5.2 Hz), 3.643.57 (m, 2H), 3.223.16 (m, 2H), 3.153.1 (m, 2H), 3.153.04 (m, 6H), 2.49–2.44 (m, 6H), 2.44–2.37 (m, 4H), 2.3 (t, 2H, J = 7.0 Hz), 2.09 (t, 4H, J = 7.4 Hz), 1.89–1.84 (m, 2H), 1.70–1.64 (m, 2H), 1.58–1.51 (m, 6H), 1.38–1.31 (m, 4H).

ESI-MS (m/z) calculated for $C_{26}H_{46}N_4O_5S_4$ $(M)^+$ 622.2; found 622.3.

The reaction yield is ~50%.

bis(LA)-*N*,*N*-dimethyl alkyl amide

^{1}H NMR (600 MHz, DMSO-d_6): δ 7.72 (t, 3H, J = 5.5 Hz), 3.643.57 (m, 2H), 3.22–3.16 (m, 2H), 3.15–3.10 (m, 2H), 3.10–3.05 (m, 6H), 2.46 (t, 6H, J = 6.5 Hz), 2.44–2.38 (m, 2H), 2.18–2.16 (t, 2H, J = 7.2 Hz), 2.10 (s, 6H), 2.10–2.07 (t, 6H, J = 7.6 Hz), 1.9–1.83 (m, 2H), 1.7–1.63 (m, 2H), 1.64–1.59 (m, 2H), 1.57–1.47 (m, 6H), 1.4–1.30 (m, 4H).

ESI-MS (m/z) calculated for $C_{28}H_{53}N_5O_3S_4$ $(M+H)^+$ 636.3; found 636.3.

The reaction yield is ~65%.

bis(LA)-ZW

IR(neat): 3,404.76, 3,289.68, 3,087.30, 2,928.57, 2,857.14, 1,641.18, 1,540.08, 1,452.86, 1,339.88, 1,254.62, 1,163.43, 1,036.57, 959.25 cm^{-1}.

ESI-MS (m/z) calculated for $C_{31}H_{59}N_5O_6S_5$ $(M+H)^+$ 758.3; found 758.3.

The reaction yield is <90%.

Note: Any Supplementary Information and Source Data files are available in the online version of the paper.

ACKNOWLEDGMENTS We thank Florida State University (FSU) and the National Science Foundation (NSFCHE, no. 1058957) for financial support. We thank M. Davidson and T.A. Cross at FSU for kindly providing us with the MBP and mCherry plasmids. We also thank M. Safi for fruitful discussions.

AUTHOR CONTRIBUTIONS H.M. and G.P. conceived the ligand design and ligation strategy. N.Z. and G.P. carried out the synthesis, optimization and characterization of the compounds. N.Z., G.P. and H.M. carried out the phase transfer strategy, analytical tests, conjugation of the QDs to the proteins and the spectroscopy characterization of the conjugates. N.Z., G.P. and H.M. wrote the manuscript.

COMPETING FINANCIAL INTERESTS The authors declare no competing financial interests.

1. Michalet, X. *et al.* Quantum dots for live cells, *in vivo* imaging, and diagnostics. *Science* **307**, 538–544 (2005).
2. Kobayashi, H. *et al.* Simultaneous multicolor imaging of five different lymphatic basins using quantum dots. *Nano Lett.* **7**, 1711–1716 (2007).
3. Zrazhevskiy, P., Sena, M. & Gao, X.H. Designing multifunctional quantum dots for bioimaging, detection, and drug delivery. *Chem. Soc. Rev.* **39**, 4326–4354 (2010).
4. Kovalenko, M.V., Bodnarchuk, M.I., Zaumseil, J., Lee, J.S. & Talapin, D.V. Expanding the chemical versatility of colloidal nanocrystals capped with molecular metal chalcogenide ligands. *J. Am. Chem. Soc.* **132**, 10085–10092 (2010).
5. Mattoussi, H., Palui, G. & Na, H.B. Luminescent quantum dots as platforms for probing *in vitro* and *in vivo* biological processes. *Adv. Drug Deliv. Rev.* **64**, 138–166 (2012).
6. Larson, D.R. *et al.* Water-soluble quantum dots for multiphoton fluorescence imaging *in vivo*. *Science* **300**, 1434–1436 (2003).
7. Kim, S. *et al.* Near-infrared fluorescent type II quantum dots for sentinel lymph node mapping. *Nat. Biotechnol.* **22**, 93–97 (2004).
8. Palui, G. *et al.* Photoinduced phase transfer of luminescent quantum dots to polar and aqueous media. *J. Am. Chem. Soc.* **134**, 16370–16378 (2012).
9. Murray, C.B., Norris, D.J. & Bawendi, M.G. Synthesis and characterization of nearly monodisperse CdE (E = S, SE, TE) semiconductor nanocrystallites. *J. Am. Chem. Soc.* **115**, 8706–8715 (1993).
10. Peng, Z.A. & Peng, X.G. Formation of high-quality CdTe, CdSe, and CdS nanocrystals using CdO as precursor. *J. Am. Chem. Soc.* **123**, 183–184 (2001).
11. Hines, M.A. & Guyot-Sionnest, P. Synthesis and characterization of strongly luminescing ZnS-Capped CdSe nanocrystals. *J. Phys. Chem.* **100**, 468–471 (1996).
12. Dabbousi, B.O. *et al.* (CdSe)ZnS core-shell quantum dots: synthesis and characterization of a size series of highly luminescent nanocrystallites. *J. Phys. Chem. B* **101**, 9463–9475 (1997).
13. Talapin, D.V., Rogach, A.L., Kornowski, A., Haase, M. & Weller, H. Highly luminescent monodisperse CdSe and CdSe/ZnS nanocrystals synthesized in a hexadecylamine-trioctylphosphine oxide-trioctylphospine mixture. *Nano Lett.* **1**, 207–211 (2001).
14. Choi, H.S. *et al.* Renal clearance of quantum dots. *Nat. Biotechnol.* **25**, 1165–1170 (2007).
15. Choi, H.S. *et al.* Design considerations for tumour-targeted nanoparticles. *Nat. Nanotechnol.* **5**, 42–47 (2010).
16. Chauhan, V.P. *et al.* Normalization of tumour blood vessels improves the delivery of nanomedicines in a size-dependent manner. *Nat. Nanotechnol.* **7**, 383–388 (2012).
17. Gerion, D. *et al.* Synthesis and properties of biocompatible water-soluble silica-coated CdSe/ZnS semiconductor quantum dots. *J. Phys. Chem. B* **105**, 8861–8871 (2001).
18. Uyeda, H.T., Medintz, I.L., Jaiswal, J.K., Simon, S.M. & Mattoussi, H. Synthesis of compact multidentate ligands to prepare stable hydrophilic quantum dot fluorophores. *J. Am. Chem. Soc.* **127**, 3870–3878 (2005).
19. Wang, M.F. *et al.* Water-soluble CdSe quantum dots passivated by a multidentate diblock copolymer. *Macromolecules* **40**, 6377–6384 (2007).
20. Liu, W. *et al.* Compact biocompatible quantum dots functionalized for cellular imaging. *J. Am. Chem. Soc.* **130**, 1274–1284 (2008).
21. Susumu, K., Mei, B.C. & Mattoussi, H. Multifunctional ligands based on dihydrolipoic acid and polyethylene glycol to promote biocompatibility of quantum dots. *Nat. Protoc.* **4**, 424–436 (2009).
22. Liu, D. & Snee, P.T. Water-soluble semiconductor nanocrystals cap exchanged with metalated ligands. *ACS Nano* **5**, 546–550 (2010).
23. Winnik, F.M. & Maysinger, D. Quantum dot cytotoxicity and ways to reduce it. *Acc. Chem. Res.* **46**, 672–680 (2013).
24. Susumu, K. *et al.* Multifunctional compact zwitterionic ligands for preparing robust biocompatible semiconductor quantum dots and gold nanoparticles. *J. Am. Chem. Soc.* **133**, 9480–9496 (2011).
25. Mattoussi, H. *et al.* Self-assembly of CdSe-ZnS quantum dot bioconjugates using an engineered recombinant protein. *J. Am. Chem. Soc.* **122**, 12142–12150 (2000).
26. Susumu, K. *et al.* Enhancing the stability and biological functionalities of quantum dots via compact multifunctional ligands. *J. Am. Chem. Soc.* **129**, 13987–13996 (2007).
27. Stewart, M.H. *et al.* Multidentate poly(ethylene glycol) ligands provide colloidal stability to semiconductor and metallic nanocrystals in extreme conditions. *J. Am. Chem. Soc.* **132**, 9804–9813 (2010).
28. Muro, E. *et al.* Small and stable sulfobetaine zwitterionic quantum dots for functional live-cell imaging. *J. Am. Chem. Soc.* **132**, 4556–4557 (2010).
29. Yildiz, I., McCaughan, B., Cruickshank, S.F., Callan, J.F. & Raymo, F.M. Biocompatible CdSe-ZnS core-shell quantum dots coated with hydrophilic polythiols. *Langmuir* **25**, 7090–7096 (2009).
30. Yildiz, I. *et al.* Hydrophilic CdSe-ZnS core-shell quantum dots with reactive functional groups on their surface. *Langmuir* **26**, 11503–11511 (2010).
31. Liu, W.H. *et al.* Compact biocompatible quantum dots via RAFT-mediated synthesis of imidazole-based random copolymer ligand. *J. Am. Chem. Soc.* **132**, 472–483 (2010).
32. Palui, G., Na, H.B. & Mattoussi, H. Poly(ethylene glycol)-based multidentate oligomers for biocompatible semiconductor and gold nanocrystals. *Langmuir* **28**, 2761–2772 (2012).

33. Delgado, C., Francis, G.E. & Fisher, D. The uses and properties of PEG-linked proteins. *Crit. Rev. Ther. Drug* **9**, 249–304 (1992).
34. Park, K.D. *et al.* Bacterial adhesion on PEG modified polyurethane surfaces. *Biomaterials* **19**, 851–859 (1998).
35. Mei, B.C., Susumu, K., Medintz, I.L. & Mattoussi, H. Polyethylene glycol–based bidentate ligands to enhance quantum dot and gold nanoparticle stability in biological media. *Nat. Protoc.* **4**, 412–423 (2009).
36. Palui, G., Aldeek, F., Wang, W.T. & Mattoussi, H. Strategies for interfacing inorganic nanocrystals with biological systems based on polymer-coating. *Chem. Soc. Rev.* **44**, 193–227 (2015).
37. Medintz, I.L. *et al.* Self-assembled nanoscale biosensors based on quantum dot FRET donors. *Nat. Mater.* **2**, 630–638 (2003).
38. Dif, A.l. *et al.* Small and stable peptidic PEGylated quantum dots to target polyhistidine-tagged proteins with controlled stoichiometry. *J. Am. Chem. Soc.* **131**, 14738–14746 (2009).
39. Ladd, J., Zhang, Z., Chen, S., Hower, J.C. & Jiang, S. Zwitterionic polymers exhibiting high resistance to nonspecific protein adsorption from human serum and plasma. *Biomacromolecules* **9**, 1357–1361 (2008).
40. Zhan, N.Q., Palui, G., Safi, M., Ji, X. & Mattoussi, H. Multidentate zwitterionic ligands provide compact and highly biocompatible quantum dots. *J. Am. Chem. Soc.* **135**, 13786–13795 (2013).
41. Zhan, N. *et al.* Combining ligand design with photoligation to provide compact, colloidally stable, and easy to conjugate quantum dots. *ACS Appl. Mater. Interfaces* **5**, 2861–2869 (2013).
42. Reiss, P., Bleuse, J. & Pron, A. Highly luminescent CdSe/ZnSe core/shell nanocrystals of low size dispersion. *Nano Lett.* **2**, 781–784 (2002).
43. Clapp, A.R., Goldman, E.R. & Mattoussi, H. Capping of CdSe-ZnS quantum dots with DHLA and subsequent conjugation with proteins. *Nat. Protoc.* **1**, 1258–1266 (2006).
44. Talapin, D.V., Lee, J.S., Kovalenko, M.V. & Shevchenko, E.V. Prospects of colloidal nanocrystals for electronic and optoelectronic applications. *Chem. Rev.* **110**, 389–458 (2010).
45. Dahan, M. *et al.* Diffusion dynamics of glycine receptors revealed by single-quantum dot tracking. *Science* **302**, 442–445 (2003).
46. Park, J. *et al.* Compact and stable quantum dots with positive, negative, or zwitterionic surface: specific cell interactions and non-specific adsorptions by the surface charges. *Adv. Funct. Mater.* **21**, 1558–1566 (2011).
47. Zhan, N., Palui, G., Grise, H. & Mattoussi, H. in *Quantum Dots: Applications in Biology*, Vol. 1199 (eds. Fontes, A. & Santos, B.S.) 13–31 (Springer, 2014).
48. Aldeek, F., Safi, M., Zhan, N.Q., Palui, G. & Mattoussi, H. Understanding the self-assembly of proteins onto gold nanoparticles and quantum dots driven by metal-histidine coordination. *ACS Nano* **7**, 10197–10210 (2013).
49. Delehanty, J.B. *et al.* Spatiotemporal multicolor labeling of individual cells using peptide-functionalized quantum dots and mixed delivery techniques. *J. Am. Chem. Soc.* **133**, 10482–10489 (2011).
50. Medintz, I.L. *et al.* Quantum-dot/dopamine bioconjugates function as redox coupled assemblies for *in vitro* and intracellular pH sensing. *Nat. Mater.* **9**, 676–684 (2010).
51. Anikeeva, N. *et al.* Quantum dot/peptide-MHC biosensors reveal strong CD8-dependent cooperation between self and viral antigens that augment the T cell response. *Proc. Natl. Acad. Sci. USA* **103**, 16846–16851 (2006).
52. Susumu, K., Uyeda, H.T., Medintz, I.L. & Mattoussi, H. Design of biotin-functionalized luminescent quantum dots. *J. Biomed. Biotechnol.* **2007**, 90651 (2007).
53. Aldeek, F. *et al.* UV and sunlight driven photoligation of quantum dots: understanding the photochemical transformation of the ligands. *J. Am. Chem. Soc.* **137**, 2704–2714 (2015).
54. Sapsford, K.E. *et al.* Kinetics of metal-affinity driven self-assembly between proteins or peptides and CdSe-ZnS quantum dots. *J. Phys. Chem. C* **111**, 11528–11538 (2007).
55. Lakowicz, J.R. *Principles of Fluorescence Spectroscopy,* 3rd edn. (Springer, 2006).
56. Clapp, A.R. *et al.* Fluorescence resonance energy transfer between quantum dot donors and dye-labeled protein acceptors. *J. Am. Chem. Soc.* **126**, 301–310 (2004).
57. Mattoussi, H., Cumming, A.W., Murray, C.B., Bawendi, M.G. & Ober, R. Properties of CdSe nanocrystal dispersions in the dilute regime: structure and interparticle interactions. *Phys. Rev. B* **58**, 7850–7863 (1998).
58. Dennis, A.M. & Bao, G. Quantum dot–fluorescent protein pairs as novel fluorescence resonance energy transfer probes. *Nano Lett.* **8**, 1439–1445 (2008).
59. Medintz, I.L. *et al.* Resonance energy transfer between luminescent quantum dots and diverse fluorescent protein acceptors. *J. Phys. Chem. C.* **113**, 18552–18561 (2009).
60. Ye, L. *et al.* A pilot study in non-human primates shows no adverse response to intravenous injection of quantum dots. *Nat. Nanotechnol.* **7**, 453–458 (2012).
61. Pons, T. & Mattoussi, H. Investigating biological processes at the single molecule level using luminescent quantum dots. *Ann. Biomed. Eng.* **37**, 1934–1959 (2009).